

Article

Z,E-Isomerism in a Series of Substituted Iminophosphonates: Quantum Chemical Research

Alexander B. Rozhenko ^{1,2,*}, Andrey A. Kyrylchuk ¹, Yuliia O. Lapinska ², Yuliya V. Rassukana ^{1,2}, Vladimir V. Trachevsky ^{1,3}, Volodymyr V. Pirozhenko ¹, Jerzy Leszczynski ⁴ and Petro P. Onysko ^{1,*}

¹ Institute of Organic Chemistry of the National Academy of Sciences of Ukraine, Murmans'ka Str. 5, 02094 Kyiv, Ukraine; kyrylchuk@ioch.kiev.ua (A.A.K.); juravi@ioch.kiev.ua (Y.V.R.); trachev@imp.kiev.ua (V.V.T.); pirozhenko@ioch.kiev.ua (V.V.P.)

² National Technical University of Ukraine "Kyiv Polytechnic Institute named after Igor Sikorsky", Peremogy Ave. 37, 03056 Kyiv, Ukraine; yuliia.shn@gmail.com

³ Technical Center of the National Academy of Sciences of Ukraine, Pokrovs'ka Str. 13, 04070 Kyiv, Ukraine

⁴ Department of Chemistry and Biochemistry, Jackson State University, Jackson, MS 39217, USA; jerzy@icnanotox.org

* Correspondence: rozhenko@ioch.kiev.ua (A.B.R.); onysko@ioch.kiev.ua (P.P.O.); Tel.: +380-44-499-4610 (A.B.R.); +380-44-573-2594 (P.P.O.)

Abstract: Esters of iminophosphonic acids (iminophosphonates, or IPs), including a fragment, >P(=O)-C=N, can be easily functionalized, for instance to aminophosphonic acids with a wide range of biological activity. Depending on the character of the substitution, the Z- or E-configuration is favorable for IPs, which in turn can influence the stereochemistry of the products of chemical transformations of IPs. While the Z,E-isomerism in IPs has been thoroughly studied by NMR spectroscopy, the factors stabilizing a definite isomer are still not clear. In the current work, density functional theory (DFT, using M06-2X functional) and ab initio spin-component-scaled second-order Møller–Plesset perturbation theory (SCS-MP2) calculations were carried out for a broad series of IPs. The calculations reproduce well a subtle balance between the preferred Z-configuration inherent for C-trifluoromethyl substituted IPs and the E-form, which is more stable for C-alkyl- or aryl-substituted IPs. The predicted trend of changing activation energy values agrees well with the recently determined experimental ΔG^\ddagger_{298} magnitudes. Depending on the substitution in the aromatic moiety, the Z/E-isomerization of N-aryl-substituted IPs proceeds via two types of close-in energy transition states. Not a single main factor but a combination of various contributions should be considered in order to explain the Z/E-isomerization equilibrium for different IPs.

Keywords: DFT calculations; SCS-MP2 calculations; Z,E-isomerism; iminophosphonates; thermodynamic stability



Citation: Rozhenko, A.B.; Kyrylchuk, A.A.; Lapinska, Y.O.; Rassukana, Y.V.; Trachevsky, V.V.; Pirozhenko, V.V.; Leszczynski, J.; Onysko, P.P. Z,E-Isomerism in a Series of Substituted Iminophosphonates: Quantum Chemical Research. *Organics* **2021**, *2*, 84–97. <https://doi.org/10.3390/org2020008>

Academic Editor: Tomasz K. Olszewski

Received: 8 March 2021
Accepted: 20 April 2021
Published: 23 April 2021

Publisher's Note: MDPI stays neutral with regard to jurisdictional claims in published maps and institutional affiliations.



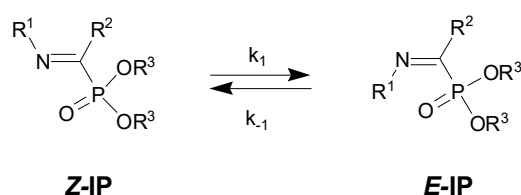
Copyright: © 2021 by the authors. Licensee MDPI, Basel, Switzerland. This article is an open access article distributed under the terms and conditions of the Creative Commons Attribution (CC BY) license (<https://creativecommons.org/licenses/by/4.0/>).

1. Introduction

Aminophosphonic acids, as phosphorus analogs of amino acids, are biologically persistent analogues of unstable tetrahedral carbon intermediates formed in enzymatic processes, and therefore act as enzyme inhibitors [1]. Derivatives of aminophosphonic acids are widely used as antibacterial, anticancer and antiviral drugs, herbicides, and enzyme regulators, etc. [1–3].

Esters of iminophosphonic acids or iminophosphonates (IPs) include an 'oxidized' fragment of aminophosphonic acids (>P(=O)-C=N), which can easily be functionalized. Therefore, they are convenient precursors in the synthesis of aminophosphonic acids, as well as a wide range of other biologically active compounds. Fluorine-substituted IPs deserve special attention because the introduction of fluorine into the molecule is not always an easy task. At the same time, the presence of fluorine atoms in the molecule significantly affects its chemical, physicochemical and pharmacological properties [4,5].

Similarly to other imines, E/Z-isomerism is inherent for IPs (Scheme 1). Two main mechanisms of isomerization are discussed in the literature: an imino-nitrogen inversion in a plane through a transition state (TS) with a CNX bond angle $\approx 180^\circ$ and a rotational process, wherein the substituent X in the TS is out of the plane with the CNX bond angle $< 180^\circ$ (Figure 1) [6,7]. It should be noted that, at present, there are no unambiguous experimental criteria for assigning the mechanism of isomerization to inversion or rotation. However, as shown by our quantum chemical study of quinonimines [7], a mixed isomerization mechanism including the rotation component in the process of inversion is realized only under certain conditions, and is determined mainly by the steric influence of the neighboring substituents. One year later, Gálvez and Guirado [8] have reported on the similar mixed isomerization mechanism in other imine derivatives. Moreover, according to [8], electron acceptor substituents determine the inversion mechanism for the isomerization, whereas the electron donor groups contribute to the rotational one. This conclusion is also consistent with the data of earlier works [9,10].



Scheme 1. Z/E isomerization of IPs.

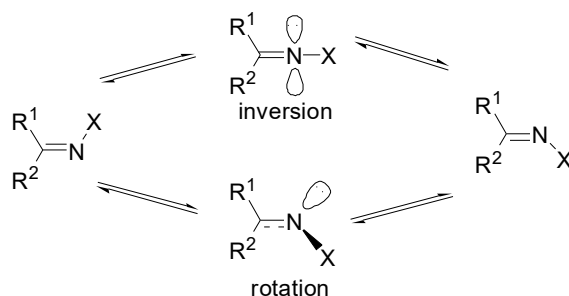


Figure 1. Two possible mechanisms of the Z/E-isomerization of imines.

IPs can exist as an equilibrium of E- and Z-isomers (Table 1) [9]. The assignment of IPs to Z- or E-isomers has recently been performed by means of ^{19}F and ^{31}P NMR spectroscopy [9,11,12]. The resonance signals of phosphorus and fluorine nuclei in Z-isomers of IPs ($\delta\text{P} - 0.1$ – 3.3 ppm, $\delta\text{F} - 66.2$ – 70.2 ppm) are high-field shifted compared to the corresponding E-isomers ($\delta\text{P} 1.5$ – 4.9 ppm, $\delta\text{F} - 61$ – 62 ppm) [9,11–13]. Structural features, the charge distribution in the molecules, electronic interactions, and reaction paths are traditional subjects of quantum chemistry investigations. Recently, we published the first example of quantum chemical calculations for the process of the Z/E-isomerization of IPs [14]. Theoretical studies of the same process have previously been performed for other substituted imines [7,8]. The isomeric ratio is determined by the nature of the substituents at the C = N double bond, and the decisive contribution to the stability of each of the isomers belongs to the substituent R^2 (Scheme 1). Thus, it is known that most derivatives with $\text{R}^2 = \text{aryl}$ exist mainly in the E-form [$\text{Z/E} \approx 1:(12\text{--}20)$], while IPs with fluoroalkyl R^2 groups are preferably Z-isomers [$\text{Z/E} \approx (6\text{--}10):1$] (Table 1). The variation of the alkyl substituent R^3 in the phosphoryl group has little effect, while the nature of the fluoroalkyl group R^2 can significantly influence the Z/E-isomeric ratio for IPs. Interestingly, in the more stable Z-isomer of trifluoromethyl-substituted IPs, the substituent R^1 at the nitrogen atom is in the cis-position relative to the bulky dialkylphosphonyl group, i.e., the sterically less-favorable isomer is more advantageous. In turn, the structure of these compounds

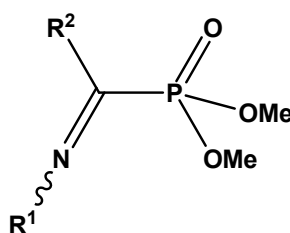
can significantly affect their chemical properties: their reactivity and the stereochemical outcome of enantio- and diastereoselective reactions, etc.

Table 1. The ratio of isomers of iminophosphonates (see Scheme 1).

Entry	R ¹	R ²	R ³	Z/E	ΔG(Z/E) ^a
1	H	CF ₃	Et	10:1 [12]	
2	H	CHF ₂	Et	5:1	
3	H	C ₃ F ₇	Et	20:1	
4	Ph	CF ₃	Et	7:1	−16.0
5	4-MeOC ₆ H ₄	CF ₃	Me	5:1 [9]	−14.4
6	4-CNC ₆ H ₄	CF ₃	Me	7:1 [9]	−19.7
7	Me	CF ₃	Et	10:1	
8	cyc-Pr	CF ₃	Et	11:1 [11]	−5.9
9	Me	Ph	Et	1:17 [9]	
10	CHMe ₂	Ph	Et	1:20	
11	4-MeOC ₆ H ₄	Ph	Et	1:13	

^a Calculated (M06-2X/6-311+G**, PCM solvent model, solvent: toluene) difference in Gibbs free energy (kJ mol^{−1}) between E and Z isomers. Negative values mean a higher stability of the Z-isomer.

In this work, we investigated Z/E-isomerism for IPs **1–10** using density functional theory (DFT) (M06-2X/6-311+G** level) and ab initio spin-component-scaled second-order Møller–Plesset perturbation theory (SCS-MP2/cc-pVTZ level) calculations [15,16] (Figure 2). In particular, the stability of the structures corresponding to the local energy minima and transition states for the Z/E-isomerization process, their relative energies, charge distribution, and bond critical points will be discussed in detail.



1 (R¹ = Me; R² = CF₃); **2** (R¹ = cyc-Pr; R² = CF₃); **3** (R¹ = R² = Me); **4** (R¹ = R² = Ph); **5** (R¹ = Ph; R² = CF₃); **6** (R¹ = p-NCC₆H₄; R² = CF₃); **7** (R¹ = p-MeOC₆H₄; R² = CF₃); **8** (R¹ = H; R² = CF₃); **9** (R¹ = H; R² = Ph); **10** (R¹ = SiMe₃; R² = CF₃)

Figure 2. Calculated iminophosphonates **1–10**.

2. Methods of Calculations

All of the calculations were performed with the GAUSSIAN-09 set of programs [17]. The M062X [15,16] function in combination with 6–31+G** basis sets [18,19] were used for the geometry optimization and calculations of the vibrational frequencies. The equilibrium structures were utilized for the generation of the PROAIMS wave function files (wfn) at the RHF/6–31G* level of theory. NBO charges were derived using the NBO 3.1 procedure [20–22] implemented into the GAUSSIAN-09 set of programs at the M062X/6–311 + G** level of approximation. The same level of theory was used for the single-point energy calculations in combination with the PCM [23] and CPCM [24,25] solvent models, as implemented into the GAUSSIAN-09 package (see ESI, Table S3). The Jmol program [26,27] was used for the graphical presentation of the structures. Single-point MP2 energy calculations for **5–7** were carried out using the TURBOMOLE program package (version 6.4) [28,29] and SCS-MP2 level of approximation [30–33] with triple-zeta cc-pVTZ Dunning's basis sets [34]. Resolution of the Identity (RI) approximation [35,36] was utilized in all cases to increase the calculation speed and efficiency. Topological Bader's 'atoms in the

molecule' (AIM) [37] and Non-Covalent Interactions (NCI) analyses [38] were performed using the Multiwfn program [39]. The energies of the hydrogen bonds were estimated according to the values of the potential energy at the critical points [40].

3. Results

The structures of the Z- and E-isomers of N-methyl derivative **1** (respectively, **1-Z** and **1-E**) and the transition state of the isomerization reaction (**1-TS**) optimized in the approximation M06-2X/6-311+G** are shown in Figure 3.

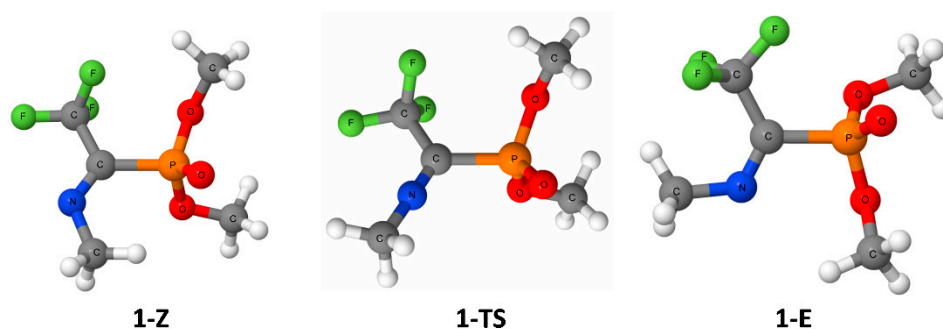


Figure 3. Optimized structures of the Z- and E-isomers (**1-Z** and **1-E**, respectively), and the transition state of the isomerization reaction **1-Z** → **1-E** (**1-TS**). Hereinafter, the structures are presented using the Jmol program [26,27,41].

Our calculations predict higher thermodynamic stability for the Z-structure of **1** (**1-Z**) (by 8.8 kJ mol⁻¹) compared to the E-form (**1-E**) (Table S1). The calculated values of the activation energies for the E→Z (ΔG) and Z→E transformations ($\Delta G'$) are 83.0 and 91.8 kJ mol⁻¹, respectively. However, the data of quantum chemical calculations do not allow us to find a trivial explanation of the observed advantage of the Z-isomer over the E-form. In particular, the Z-structure seems to be stabilized by two hydrogen bonding (HB) H...F (2.410 Å) and H...O (2.532 Å). These are confirmed by the existence of corresponding (3, -1) critical points (CPs) obtained by the analysis of the electron density by Bader's 'atoms in the molecule' method (AIM) [37] (Figure 4, left, CPs 1 and 2). The estimated energies of the hydrogen bonding [40] are -10.2 and -10.6 kJ mol⁻¹, respectively. However, the corresponding energies of the three HBs H...N (2.745 Å) and H...F (2.407 and 2.408 Å) found in **1-E** (Figure 4, right) for CPs 1, 2 and 3 (-6.9, -11.5 and -12.9 kJ mol⁻¹, respectively) in total even exceed the energy of the HBs in the more favorable **1-Z** structure. Therefore, hydrogen bonding by itself does not explain the higher thermodynamic stability of the **1-Z** structure compared to **1-E**. No new conclusions can be drawn either from the analysis of the NBO charge distributions in either isomers (Figure 5). For example, the favorable Coulomb interaction (C^{δ-}H₃-C^{δ+}F₃) could rather be expected for **1-E**, whereas for the more stable **1-Z**, the similar charge configuration C^{δ-}H₃-P^{δ+} is identical to that predicted for the equilibrium structure of the less favorable **3-Z** isomer without the trifluoromethyl group (*vide infra*).

The replacement of the methyl substituent with the cyclopropyl group (Figure 6, structures **2-E** and **2-Z**, models of the real compound, see Table 1, entry 8) does not provide significant changes in the relative stability of the isomers: the structure of **2-E** is still noticeably (7.5 kJ mol⁻¹) less favorable than the **2-Z** isomer. The only structural feature is a conformational isomerism due to the rotation of the cyc-Pr substituent: in the most advantageous structure, the hydrogen atom N-CH forms an HB with P = O oxygen of the phosphonyl group (Z-isomer), or with the fluorine atom (E-isomer) (Figure 6). The calculated ΔG and $\Delta G'$ values (**2-E**→**2-Z** ΔG 78.4 kJ mol⁻¹, **2-Z**→**2-E** $\Delta G'$ 86.5 kJ mol⁻¹) are slightly lower than the corresponding values predicted for the isomerization process of methyl derivative **1** (see above). At first sight, the transition state structure **2-TS** could be stabilized via two weak C-F...H-C hydrogen bonds, and electron density distribution analysis using the NCI method [38] indicated weak attraction between fluorine and hydrogen

atoms (see ESI, Figure S1, left). However, the absence of the corresponding bond-critical points in the AIM analysis (Figure S1, right) does not support this assumption.

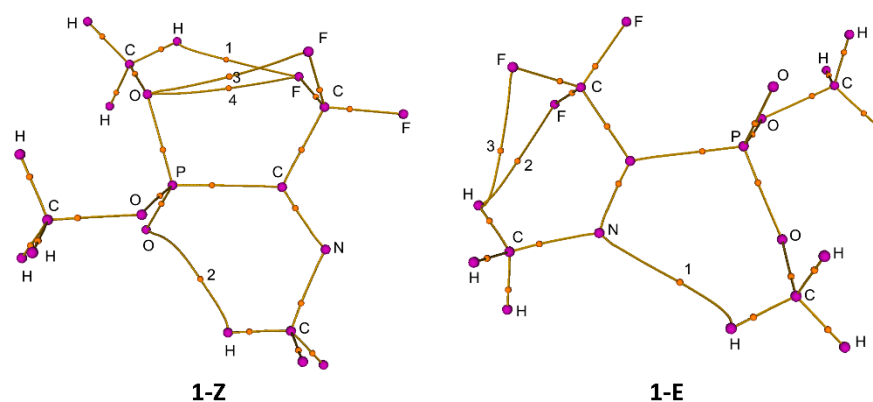


Figure 4. Bond-critical points of type (3, -1) (CPs) for 1-Z and 1-E.

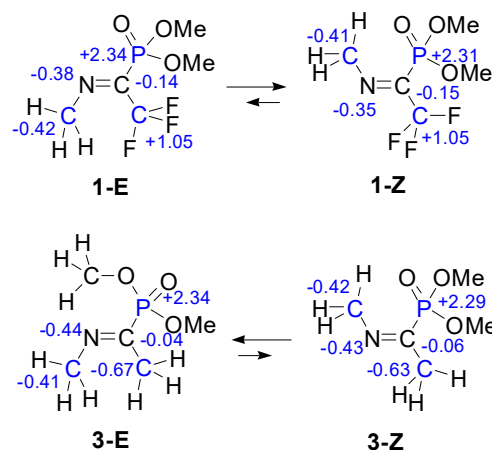


Figure 5. Charges on the atoms in compounds 1 and 3, calculated by the NBO method.

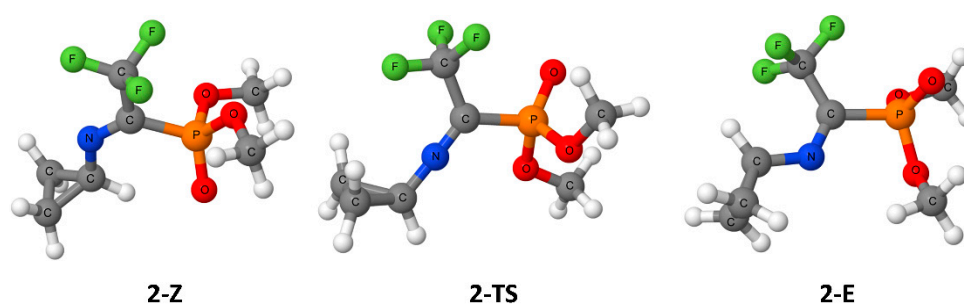


Figure 6. Optimized structures of Z- and E-isomers (2-Z and 2-E, respectively) and the transition state of the isomerization reaction 2-Z → 2-E (2-TS).

In contrast to compounds 1 and 2, for methyl derivative 3 (Figure 7), the 3-E isomer proved to be more stable than the corresponding 3-Z structure by 4.6 kJ mol^{-1} , and the inversion barriers increased sharply (3-E → 3-Z ΔG $102.0 \text{ kJ mol}^{-1}$, $\Delta G'$ 3-Z → 3-E 97.4 kJ mol^{-1}). The only important difference in the charge distribution in the molecule, compared to 1, is the lack of a positive charge on the carbon atom of the methyl group, which replaces the CF_3 group (Figure 5). The close proximity of the similarly charged carbon atoms in 3E should destabilize the more stable E-structure compared with the Z-isomer. Thus, the different charge distributions in 1 and 3 that influence the Coulomb interactions in the

isomeric structures cannot serve as a suitable explanation for the configurational stability in the series of interest.

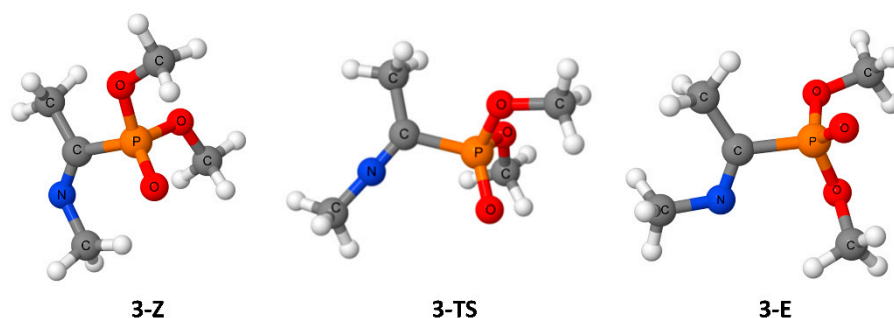


Figure 7. Optimized structures of Z- and E-isomers (3-Z and 3-E, respectively) and the transition state of the isomerization reaction 3-Z \rightarrow 3-E (3-TS).

The replacement of C- and N-methyl groups in **3** by phenyl substituents (Figure 8, structures 4-Z and 4-E) decreases the advantage for the 4-E-isomer to 1.7 kJ mol⁻¹. Therefore, the theoretically and experimentally found stabilization of the Z-isomers in compounds **1,2** is mainly an effect of the trifluoromethyl group. The values of the activation energy for the isomerization processes E \rightarrow Z (ΔG) and Z \rightarrow E ($\Delta G'$) for compound **4** are lower than those found for **1**: 62.1 and 60.4 kJ mol⁻¹, respectively (Table S1). The lower activation barriers can probably be referred to an additional stabilization of the 4-TS transition state by conjugation effects.

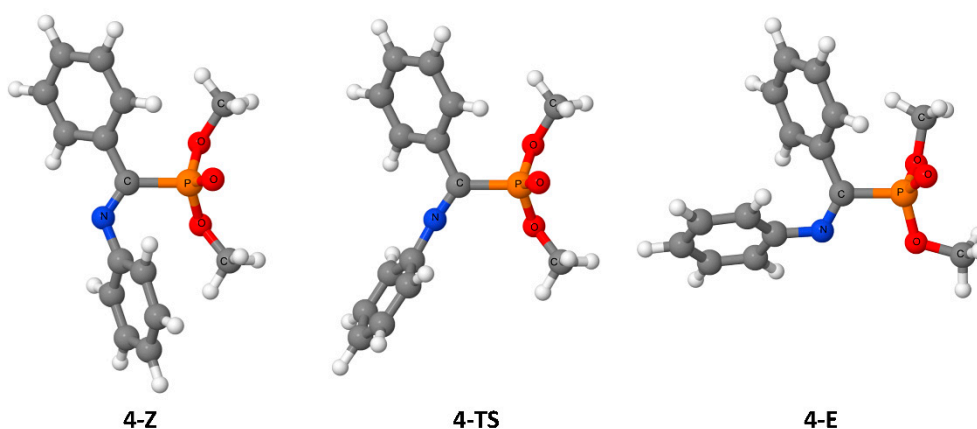


Figure 8. Optimized structures of Z- and E-isomers (4-Z and 4-E, respectively) and the transition state of the isomerization reaction 4-Z \rightarrow 4-E (4-TS).

Previously [9], we investigated the process of Z/E-isomerization in N-aryltrifluoroacetimidoyl phosphonates by dynamic NMR on ¹⁹F nuclei, and we calculated the rate constant of the isomerization process and its thermodynamic parameters using the Eyring equation. The activation barriers for the transformation were found to be quite low, such that it proceeds even at room temperature [9]. For model **5** (Figure 9), our calculations predict conformational isomerism for the structures corresponding both to the local energy minima and to TS structures. As our calculations show, it is possible to localize for **5** two different energy minima for the E-forms, 5-E and 5'-E (5'-E is 6.2 kJ mol⁻¹ more stable than 5-E), and the geometry of the corresponding Z-isomers, 5-Z and 5'-Z differs, too (5-Z is 5.7 kJ mol⁻¹ more stable than 5'-Z and 9.2 kJ mol⁻¹ more stable than 5'-E). The structure of 5-Z seems to be stabilized due to CH, π -interactions: the distance from one of the hydrogen atoms of the P-methoxy group to the carbon atoms of the Ph ring is almost identical, 2.8–2.9 Å, while for the conformation 5'-Z C^{Ph}H...O=P, hydrogen bonding was found. For these two types of conformational isomers, two different paths of Z,E-transformation and correspondingly,

two transition state structures (**5-TS** and **5'-TS**) can be located. Interestingly, despite almost identical calculated total energies (the difference in ΔG values is only ca. 0.2 kJ mol^{-1} in favor of **5'-TS**), the structures themselves differ significantly. In the case of **5-TS**, it is easy to recognize an iminium-type structure, in which the plane of the Ph moiety and the plane of the $\text{C}=\text{N}$ π -system are almost orthogonal to each other (the corresponding dihedral angle in the optimized TS structure is $\sim 65^\circ$), which minimizes steric interactions. The alternative (and somewhat more advantageous) structure of **5'-TS** is of the quinone imine type: the two π -systems are in the same plane, and the structure is stabilized by two hydrogen bonds, $\text{F}\cdots\text{H}$ (2.78 \AA) and $\text{O}\cdots\text{H}$ (2.96 \AA). Therefore, the isomerization of **5** can proceed via two different reaction pathways, as the isomeric local minima for the most favorable **5'-E** and **5-Z** structures can easily undergo transformations to **5-E** and **5'-Z**, respectively, with much lower activation energies (not studied here in detail).

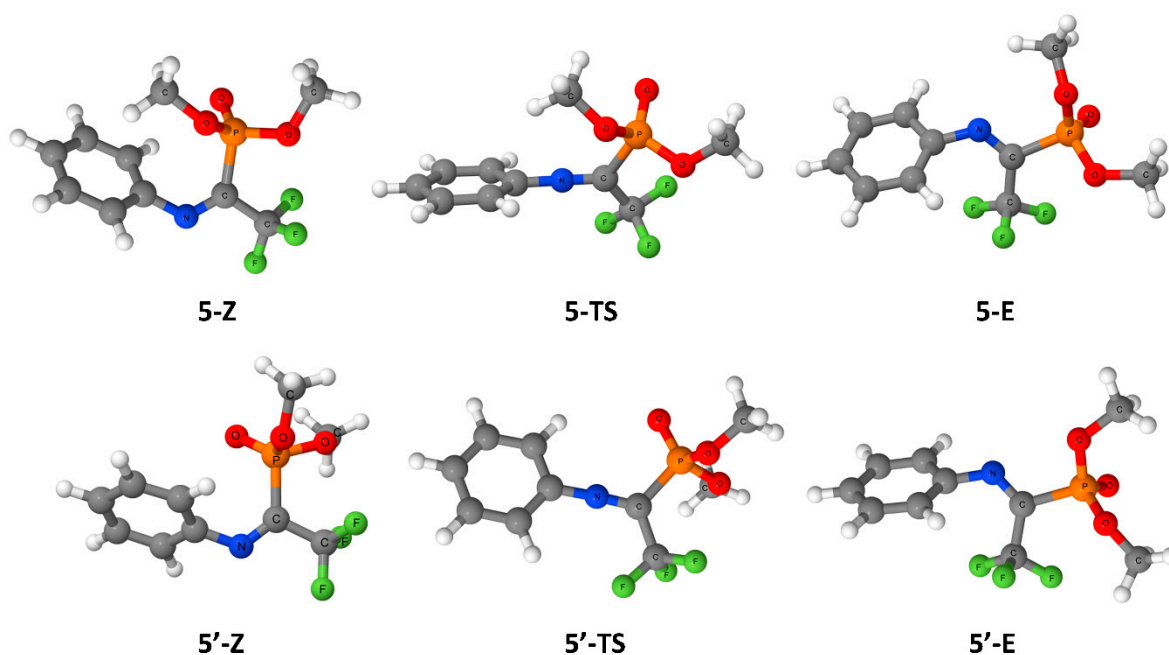


Figure 9. Optimized structures of the Z- and E-isomers of compound **5** (**5-Z**, **5'-Z** and **5-E**, **5'-E**, respectively), and the structures corresponding to the transition states of the isomerization reaction (**5-TS** and **5'-TS**).

As we have shown previously [9], the introduction of the electron acceptor substituent (CN) in the para-position of the aromatic moiety significantly accelerates the isomerization process, i.e., it reduces the activation energy of the inversion around the nitrogen atom. The DFT calculations evidence that the substitution character in the aromatic ring affects the structure of the ground and transition states (Figure 10): the only located TS structure **6-TS** involving the acceptor nitrile group mimics structure **5-TS** (Scheme 2), whereas the donor methoxy group promotes the formation of the planar transition state **7-TS**, which is similar to **5'-TS** discussed above.

The different polar structures predicted for **6-TS**, involving the imino-nitrogen lone pair in direct conjugation with the π -acceptor nitrile group, and **7-TS** with the delocalization of electron density from the π -donor methoxy oxygen onto the acceptor CF_3 and phosphonic groups (Scheme 2) is reflected in their geometry: the $\text{CF}_3\text{C-N}$ bond is slightly shorter in **6-TS** (1.228 \AA) than in **7-TS** (1.237 \AA), and the interatomic distances C-P and C-CF_3 in **6-TS** (1.858 and 1.541 \AA , respectively) are still slightly longer than those predicted for **7-TS** (1.842 and 1.534 \AA , respectively).

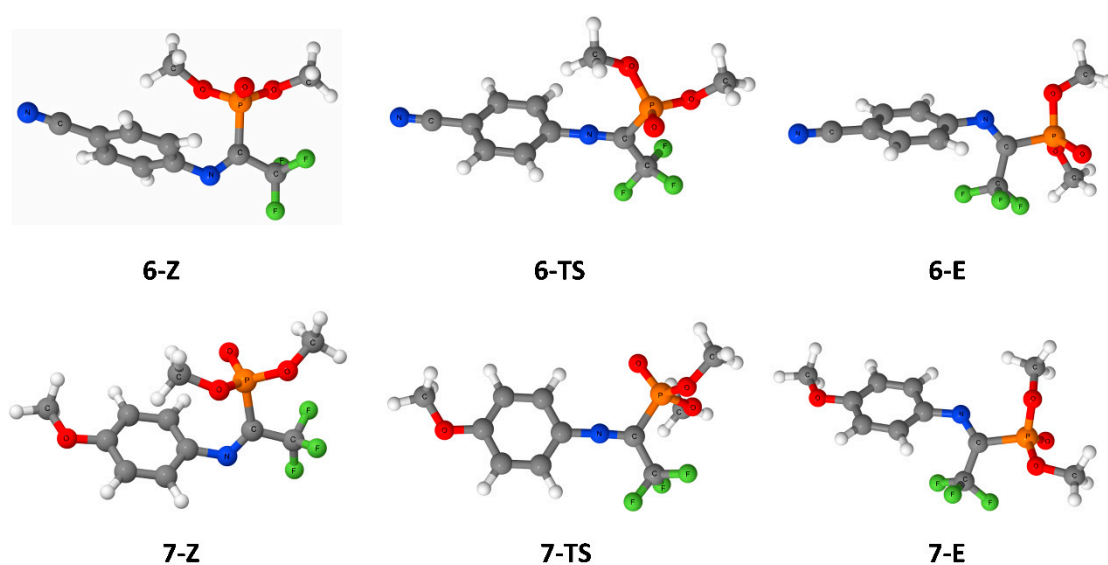
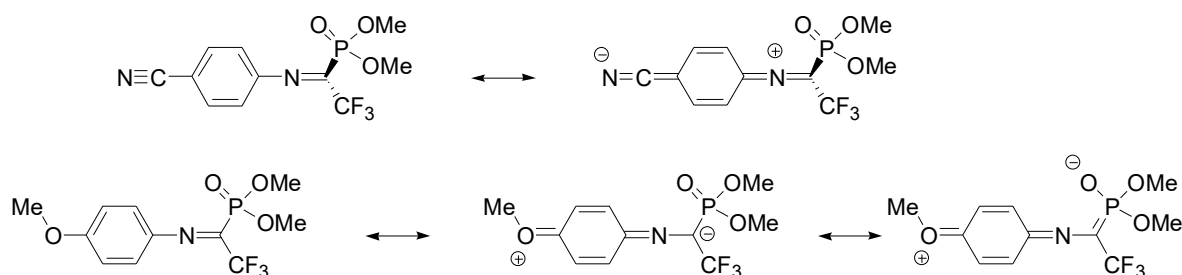


Figure 10. Optimized structures of the Z- and E-isomers of compounds 6 and 7 (6-Z, 7-Z and 6-E, 7-E, respectively), and the structures corresponding to the transition states of the isomerization reaction (6-TS and 7-TS).

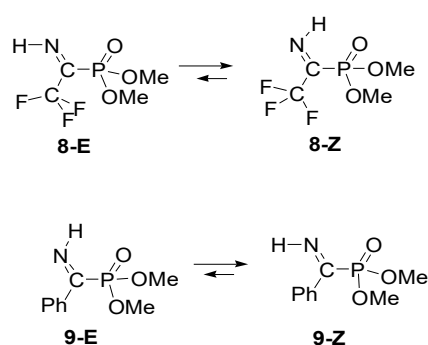


Scheme 2. Different substituent effects of electron delocalization in compounds 6 and 7, stabilizing the transition state structure for the Z,E-isomerization reaction.

It was found by a dynamic NMR study that the activation barriers of Z→E isomerization in toluene- d_8 increase in the order $6 < 5 < 7$ (ΔG^\ddagger_{298} 64.6, 67.1 and 73.4 kJ mol $^{-1}$, respectively) [9]. However, the gas phase DFT calculations failed to reproduce the experimental trend of activation energies. In particular, the activation energy calculated for Z→E isomerization in the 4-CN-substituted compound 6 (ΔG 68.3 kJ mol $^{-1}$) is even slightly higher than the value predicted for the 4-methoxy derivative 7 (ΔG 66.5 kJ mol $^{-1}$). Finally, the highest activation barrier in the studied series was predicted for phenyl derivative 5 (ΔG 73.5 kJ mol $^{-1}$). Such discrepancies were observed despite the use of the DFT functional (M06-2X), which is known to reproduce well the thermochemistry of chemical reactions and, in particular, the values of activation barriers [15,16]. As could be expected, taking into account the solvent effects for the low-polar toluene using empirical PCM and CPCM methods did not improve the compliance with the experiment (see Table S3). In particular, while some qualitative agreement was found for 5–7 between the experimentally found Z/E-isomeric ratio and the calculated differences in the Gibbs free energy values, corrected for solvent effects (Table 1, Table S3), predicting the lowest advantage of Z-isomer for 7, the predicted stability of 2-Z was obviously too low. Thus, the stability of Z-isomers seems to be overestimated for structures 5–7, and—at the chosen approximation level—we cannot expect any general correlation between the calculated and experimental data. However, the application of a more superior RI-SCS-MP2 level of approximation [33] in combination with the larger Dunning cc-pVTZ basis sets [34] and DFT corrections to ΔG values (Table S2) to some extent lowers the advantage of Z-isomers for structures 5, 6 and 7 (3.3, 13.0 and

5.3 kJ mol⁻¹, respectively), and establishes the correct ratio of activation energies for these model structures (see Discussion).

The replacement of the substituent at the nitrogen atom by hydrogen (Scheme 3) should additionally stabilize the Z-isomers compared to the E-structures due to a probable formation of N-H...O=P hydrogen bonds (Figures 11 and 12). The calculated values of activation energies ΔG related to the more stable Z-isomers **8-Z** and **9-Z** (Table S1, 107.2 and 119.7 kJ mol⁻¹, respectively) are the highest for the studied series of IPs. A suitable explanation for such high barriers, in addition to hydrogen bonding stabilizing the Z-configuration, is the small values of the $\angle\text{HNC}$ valence angle (Table S1, 109.9 and 110.7 for **8-Z** and **9-Z**, respectively), which are much smaller than the corresponding $\angle\text{CNC}$ angle of 122.0° found for the **1-Z** structure (the structure with the larger XNC bond angle is closer to the transition state structure and requires less activation energy for the inversion at nitrogen [7]).



Scheme 3. Isomerization of 8 and 9.

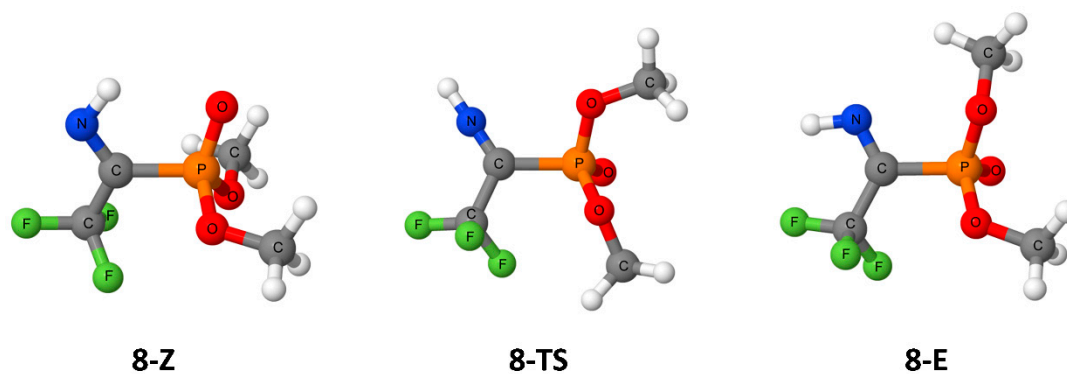


Figure 11. Optimized structures of the Z- and E-isomers of compound 8 (**8-Z** and **8-E**, respectively), and the structure corresponding to the transition state of the isomerization reaction (**8-TS**).

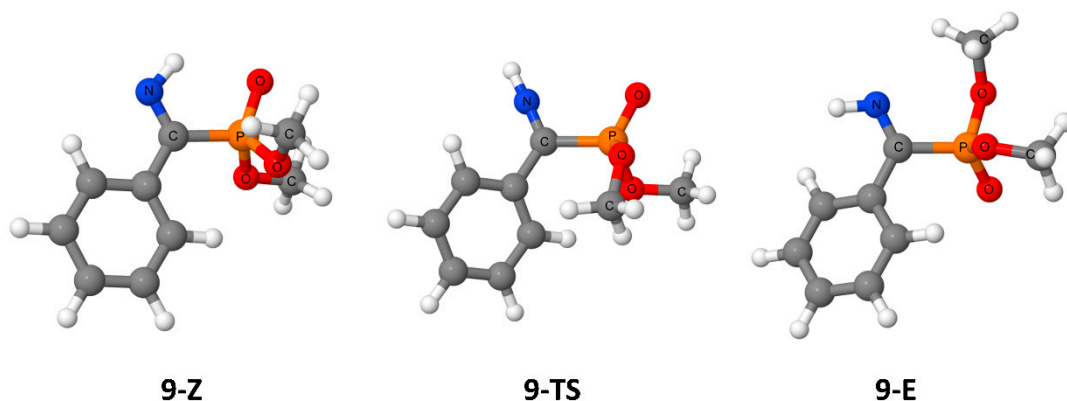
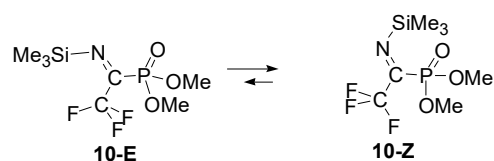


Figure 12. Optimized structures of the Z- and E-isomers of compound 9 (**9-Z** and **9-E**, respectively), and the structure corresponding to the transition state of the isomerization reaction (**9-TS**).

As evidence for this assumption, the replacement of the methyl group in **1** by a trimethylsilyl substituent (Scheme 4, structures **10**) destabilizes the ground states for both the E- and Z-isomers (Figure 13) due to the influence of steric factors. The corresponding $\angle\text{SiNC}$ bond angles (138.0 and 136.2° , respectively) significantly exceed the corresponding values in **1-E** and **1-Z** (122.8 and 122.0°), and are much closer to the geometry of the **10-TS** (Figure 13). This facilitates the Z,E-isomerization reaction [7], and determines the lowest activation energies for the **10-E**→**10-Z** (ΔG) and **10-Z**→**10-E** ($\Delta G'$) isomerization processes in the studied series of IPs (9.8 and 25.9 kJ mol^{-1} , respectively). Due to the significant difference in energy in favor of **10-Z** ($\Delta G -16.1$ kJ mol^{-1}), IP **10** will exist in a rapid dynamic equilibrium between the E- and Z-forms, strongly shifted towards the Z-isomer.



Scheme 4. Isomerization of **10**.

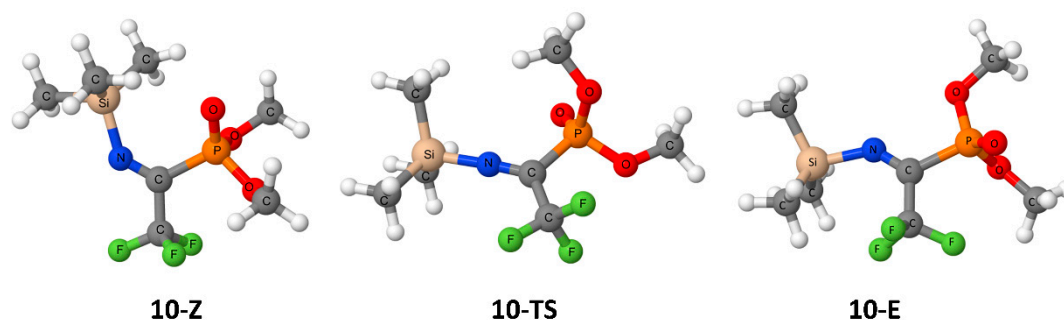
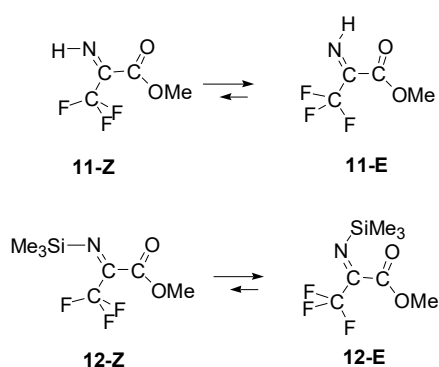


Figure 13. Optimized structures of the Z- and E-isomers of compound **10** (**10-Z** and **10-E**, respectively), and the structure corresponding to the transition states of the isomerization reaction (**10-TS**).

The replacement of the dialkylphosphonic group in **9** and **10** by the ester moiety (Scheme 5, compounds **11** and **12**, respectively) does not significantly affect the activation energies of the Z,E-isomerization process. The most stable are E-isomers **11-E** and **12-E**, which in their structure and the position of their substituents are similar to **9-Z** and **10-Z** isomers. The structure **11-E** (Figure 14), which is perfectly planar (symmetry C_s), is obviously stabilized due to the hydrogen bond $\text{N-H}\cdots\text{O}=\text{C}$, as evidenced by its short $\text{H}\cdots\text{O}$ distance (2.238 Å). Structure **11-E** is 35.9 kJ mol^{-1} more stable than **11-Z**, and the value of the activation energy of the process of Z,E-isomerization is 101.3 kJ mol^{-1} (relative to the more stable isomer **11-E**). Therefore, the presence of both isomers with a significant advantage of **11-E** should be expected both in the gas phase and in solutions (see Table S3), and rapid isomerization will not occur even at elevated temperatures. In contrast—as in the case of compound **10**—for the trimethylsilyl derivative **12** (Figure 15), the value of the activation barrier calculated at the DFT approximation level is only 24.3 kJ mol^{-1} in relation to the isomer **12-E**, which—according to the results of calculations—is more stable than **12-Z** by 13.4 kJ mol^{-1} . This agrees with the large predicted value of the $\angle\text{CNSi}$ valence angles (137.5 and 134.4° , respectively, *vide supra*).



Scheme 5. Isomerization of 11 and 12.

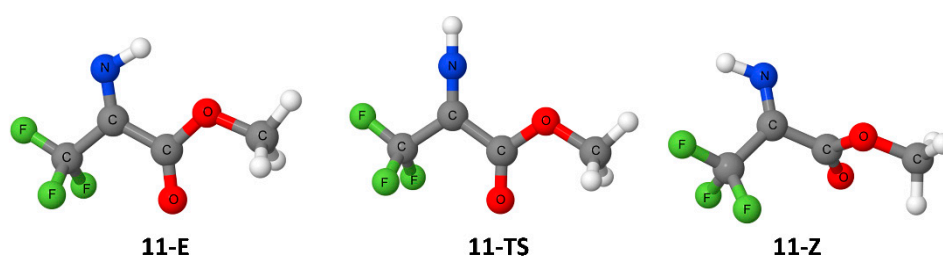


Figure 14. Optimized structures of the Z- and E-isomers of compound 11 (11-Z and 11-E, respectively), and the structure corresponding to the transition states of the isomerization reaction (11-TS).

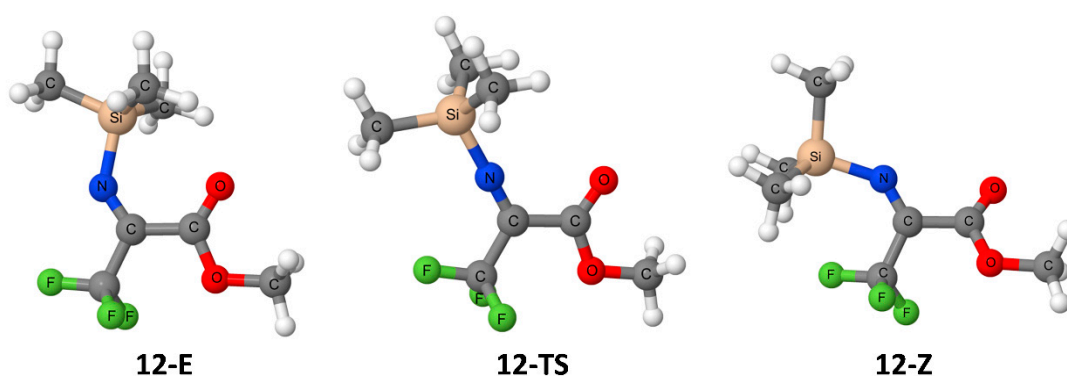


Figure 15. Optimized structures of the Z- and E-isomers of compound 12 (12-Z and 12-E, respectively), and the structure corresponding to the transition states of the isomerization reaction (12-TS).

4. Discussion

The experimentally found specific effect of the trifluoromethyl group stabilizing the sterically less-favorable Z-form of IPs is reproduced well by quantum chemical calculations. However, the key factor causing the stabilization cannot be easily identified: the driving role of hydrogen bonding (HB) in the Z-isomer of 1-Z cannot be confirmed by HB energy estimation. In addition, the AIM method unexpectedly indicates the presence of bond CPs between fluorine and oxygen atoms (Figure 4, left, critical points 3 and 4), as well as in some other CF₃-substituted IPs (see Figure S2). The calculated O⋯F interatomic distances (2.89 and 2.92 Å) are even slightly shorter than the sum of the van der Waals radii of oxygen and fluorine (2.99 Å) [33]. The found O⋯F interactions cannot be referred to the well-known ‘halogen bond’ [42–46], which withal is very rarely observed for the fluorine–oxygen pair [47]: the predicted C-F-O bond angle is far away from the favored value of 180°, which is typical for halogen bonding. Generally, the presence of CPs cannot be considered as evidence of bonding [48,49]. Thus, the found CPs could be considered as an artifacts, not manifesting true bonding between fluorine and oxygen atoms. In this case,

a steric compression of the O...F interatomic distances is unfavorable, and more likely resulted from the effect of other factors stabilizing the equilibrium conformations. This is confirmed by the NCI method [38], indicating repulsion between the fluorine and oxygen atoms (Figure S3).

It was shown that the isomerization of compounds 5–7 can pass through two different but close-in-energy TSs, having the iminium and quinone imine structures (Scheme 2). The structure of TS is determined by the nature of the substituent in the aromatic moiety. The discrepancies observed for the calculated values of the activation energies using the DFT functional (M06-2X) were overcome by performing single-point energy calculations at the more superior RI-SCS-MP2 level of approximation [33] in combination with the larger Dunning cc-pVTZ basis sets [34]. The corrections to ΔG values calculated at the DFT level of theory established the correct ratio of activation energies between 5, 6 and 7 ($\Delta G(\text{MP2})$ 73.2, 75.8 and 75.9 kJ mol⁻¹, respectively). The activation barrier predicted for the 5-TS transition state is now definitely lower than that expected for the alternative reaction pathway via the 5'-TS transition state ($\Delta\Delta G(\text{MP2})$ -5.4 kJ mol⁻¹). Therefore, the complete 5'-E to 5-Z transformation proceeds can be formulated as 5'-E → 5-E → 5-TS → 5-Z, where the conformational equilibrium in the first stage requires much less activation energy than the nitrogen inversion.

In conclusion, the structure of IPs is determined by a combination of factors such as HB, electronic and electrostatic interactions, and steric factors. In general, the advantage of Z- or E-isomers found in the experiment is well reproduced at the DFT level of theory. For the modeling of subtle substituent effects, the use of the more superior MP2 level of approximation is necessary. At the same time, the value of the activation energies is determined primarily by steric factors: the smaller the valence angle on the nominal nitrogen atom in the ground state of the compound, the higher the activation barrier for the inversion at nitrogen. Within the studied series, the values of the activation energy range from 10 to 110 kJ mol⁻¹, which corresponds to the isomerization freely proceeding at room temperature, or the simultaneous presence of both isomers in solution in the absence of rapid exchange at the temperature limit of the standard NMR probe head (~120 °C).

Supplementary Materials: The following are available online at <https://www.mdpi.com/article/10.3390/org2020008/s1>, Table S1: Calculated (M062X/6-311+G**) total energy values (E), zero-point energy correction (ZPE), thermal correction to Gibbs free energy (TCGFE), corrected energy values (E+ZPE and E+TCGFE), relative energy values (ΔE and ΔG) and the lowest vibration. Table S2: Calculated (RI-MP2/cc-pVTZ) total energy values (E(MP2)), zero point energy correction (ZPE, M062X/6-311+G**), thermal correction to Gibbs free energy (TCGFE, M062X/6-311+G**), corrected energy values (E+ZPE and E+TCGFE, without scaling), relative energy values (ΔE and ΔG), and the lowest vibration (M062X/6-311+G**). Table S3: Calculated (M062X/6-311+G**) total energy values, taking into account solvent effects (PCM and CPCM methods), zero-point energy correction (ZPE, M062X/6-311+G**), corrected energy values (E+ZPE, without scaling), and relative energy values (ΔE). Figure S1: An illustration of weak C-F...H-C attraction (green) (left) and bond critical points of type (3, -1) and (3, +1) (CPs) (right) for 2-TS structure. Figure S2: Bond-critical points of type (3, -1) and (3, +1) (CPs) for E- and Z-isomers of 1–3. Figure S3: An illustration of non-covalent interactions for compound 1-Z. The gradient isosurfaces ($s = 0.5$ a.u.) are colored on a blue-green-red scale according to the character of interaction, where blue indicates attractive interactions and red indicates strong repulsive interactions. Cartesian coordinates for equilibrium (M062X/6-311+G**) structures.

Author Contributions: Conceptualization, A.B.R., Y.V.R., V.V.T. and P.P.O.; methodology, A.B.R. and A.A.K.; software, A.B.R., A.A.K. and J.L.; validation, A.B.R., J.L. and P.P.O.; formal analysis, V.V.P., V.V.T., Y.V.R. and P.P.O.; investigation, A.A.K., V.V.P. and Y.O.L.; resources, A.B.R. and J.L.; data curation, A.B.R. and P.P.O.; writing—original draft preparation, A.B.R. and P.P.O.; writing—review and editing, A.B.R., J.L. and P.P.O.; visualization, A.B.R. and A.A.K.; supervision, A.B.R., Y.V.R. and P.P.O.; project administration, A.B.R., Y.V.R. and P.P.O.; funding acquisition, A.B.R. and P.P.O. All authors have read and agreed to the published version of the manuscript.

Funding: This research received no external funding.

Institutional Review Board Statement: Not applicable.

Informed Consent Statement: Not applicable.

Data Availability Statement: The Supplementary Materials are available online.

Acknowledgments: The authors thank Benjamin Pharr, Director of the Mississippi Center for Supercomputing Research for the computational resources and technical support for the calculations. A.R. thanks the Alexander von Humboldt foundation for purchasing the license for the TURBOMOLE program set.

Conflicts of Interest: The authors declare no conflict of interest.

References

1. Kafarski, P.; Lejczak, B. Biological activity of aminophosphonic acids. *Phosphorus Sulfur Silicon Relat. Elem.* **1991**, *63*, 193–215. [CrossRef]
2. Turcheniuk, K.V.; Kukhar, V.P.; Röschenthaler, G.-V.; Aceña, J.L.; Soloshonok, V.A.; Sorochinsky, A.E. Recent advances in the synthesis of fluorinated aminophosphonates and aminophosphonic acids. *RSC Adv.* **2013**, *3*, 6693–6716. [CrossRef]
3. Su, Q.; Li, Y.; Wang, B.; Liu, M.; Wang, H.; Wang, W.; Liu, F. Combining the Advantages of Alkene and Azo E–Z Photoisomerizations: Mechanistic Insights into Ketoimine Photoswitches. *J. Phys. Chem. A* **2017**, *121*, 2588–2596. [CrossRef]
4. Purser, S.; Moore, P.R.; Swallow, S.; Gouverneur, V. Fluorine in medicinal chemistry. *Chem. Soc. Rev.* **2008**, *37*, 320–330. [CrossRef]
5. Smart, B.E. Fluorine substituent effects (on bioactivity). *J. Fluor. Chem.* **2001**, *109*, 3–11. [CrossRef]
6. Knorr, R.; Ruhdorfer, J.; Mehlstäubl, J.; Böhrer, P.; Stephenson, D.S. (E, Z)1-Equilibria, 17 Demonstration of the Nitrogen Inversion Mechanism of Imines in a Schiff Base Model. *Eur. J. Inorg. Chem.* **1993**, *126*, 747–754. [CrossRef]
7. Pirozhenko, V.V.; Rozhenko, A.B.; Avdeenko, A.P.; Konovalova, S.A.; Santalova, A.A. Z,E-Isomerization mechanism for N-arylthio-1,4-benzoquinonimines: DNMR and DFT investigations. *Magn. Reson. Chem.* **2008**, *46*, 811–817. [CrossRef] [PubMed]
8. Gálvez, J.; Guirado, A. A theoretical study of topomerization of imine systems: Inversion, rotation or mixed mechanisms? *J. Comput. Chem.* **2009**, *31*, 520–531. [CrossRef] [PubMed]
9. Khomutnik, Y.Y.; Onys'Ko, P.P.; Rassukanaya, Y.V.; Pirozhenko, V.V.; Sinita, A.D. N-aryltrifluoroacetimidoylphosphonates. *Russ. J. Gen. Chem.* **2013**, *83*, 445–452. [CrossRef]
10. Roberts, J.D.; Hall, G.E.; Middleton, W.J. Nuclear magnetic resonance spectroscopy. Kinetics of isomerization of p-substituted hexafluoroacetone N-phenylimines. *J. Am. Chem. Soc.* **1971**, *93*, 4778–4781. [CrossRef]
11. Onys'Ko, P.P.; Klyukovskii, D.V.; Bezdudnyi, A.V.; Pirozhenko, V.V.; Pustovit, Y.M.; Synytsya, A.D. N-(R-Cyclopropyl)trifluoroacetimidoyl Phosphonates. *Phosphorus. Sulfur. Silicon Relat. Elem.* **2014**, *189*, 1094–1101. [CrossRef]
12. Onys'Ko, P.; Rassukana, Y.; Kolotylo, M.; Sinita, O.; Pirozhenko, V. α -Iminotrifluoroethylphosphonates: The First Representatives of N-H Imidoyl Phosphonates. *Synthesis* **2007**, *2007*, 2627–2630. [CrossRef]
13. Wahbi, A.; Slimani, H.; Touil, S. Multinuclear NMR structural study of novel γ -iminophosphonate and phosphine oxide derivatives. *J. Struct. Chem.* **2015**, *56*, 34–41. [CrossRef]
14. Onys'ko, P.; Chudakova, T.I.; Pirozhenko, V.V.; Rozhenko, A.B. α -Ketophosphonates in the Synthesis of α -iminophosphonates. *Curr. Green Chem.* **2020**, *7*, 226–238. [CrossRef]
15. Zhao, Y.; Truhlar, D.G. The M06 suite of density functionals for main group thermochemistry, thermochemical kinetics, noncovalent interactions, excited states, and transition elements: Two new functionals and systematic testing of four M06-class functionals and 12 other functionals. *Theor. Chem. Acc.* **2008**, *120*, 215–241. [CrossRef]
16. Zhao, Y.; Truhlar, D.G. Density Functionals with Broad Applicability in Chemistry. *Acc. Chem. Res.* **2008**, *41*, 157–167. [CrossRef]
17. Frisch, M.J.; Trucks, G.W.; Schlegel, H.B.; Scuseria, G.E.; Robb, M.A.; Cheeseman, J.R.; Scalmani, G.; Barone, V.; Mennucci, B.; Petersson, G.A.; et al. *Gaussian 09, Revision D.01*; Gaussian: Wallingford, CT, USA, 2013.
18. McLean, A.D.; Chandler, G.S. Contracted Gaussian basis sets for molecular calculations. I. Second row atoms, Z=11–18. *J. Chem. Phys.* **1980**, *72*, 5639–5648. [CrossRef]
19. Frisch, M.J.; Pople, J.A.; Binkley, J.S. Self-consistent molecular orbital methods 25. Supplementary functions for Gaussian basis sets. *J. Chem. Phys.* **1984**, *80*, 3265–3269. [CrossRef]
20. Foster, J.P.; Weinhold, F. Natural hybrid orbitals. *J. Am. Chem. Soc.* **1980**, *102*, 7211–7218. [CrossRef]
21. Reed, A.E.; Weinstock, R.B.; Weinhold, F. Natural population analysis. *J. Chem. Phys.* **1985**, *83*, 735–746. [CrossRef]
22. Reed, A.E.; Weinhold, F. Natural localized molecular orbitals. *J. Chem. Phys.* **1985**, *83*, 1736–1740. [CrossRef]
23. Scalmani, G.; Frisch, M.J. Continuous surface charge polarizable continuum models of solvation. I. General formalism. *J. Chem. Phys.* **2010**, *132*, 114110. [CrossRef]
24. Barone, V.; Cossi, M. Quantum Calculation of Molecular Energies and Energy Gradients in Solution by a Conductor Solvent Model. *J. Phys. Chem. A* **1998**, *102*, 1995–2001. [CrossRef]
25. Cossi, M.; Rega, N.; Scalmani, G.; Barone, V. Energies, structures, and electronic properties of molecules in solution with the C-PCM solvation model. *J. Comput. Chem.* **2003**, *24*, 669–681. [CrossRef]
26. Jmol: An Open-Source Java Viewer for Chemical Structures in 3D. Available online: <http://www.jmol.org/> (accessed on 21 April 2021).

27. Canepa, P.; Hanson, R.M.; Ugliengo, P.; Alfredsson, M. J-ICE: A new Jmolinterface for handling and visualizing crystallographic and electronic properties. *J. Appl. Crystallogr.* **2010**, *44*, 225–229. [CrossRef]
28. TURBOMOLE GmbH. *TURBOMOLE V6.3*, 2011, University of Karlsruhe and Forschungszentrum Karlsruhe GmbH, 1989–2007. TURBOMOLE GmbH, Since 2007. Available online: <http://www.turbomole.com> (accessed on 21 April 2021).
29. Furche, F.; Ahlrichs, R.; Hättig, C.; Klopper, W.; Sierka, M.; Weigend, F. Turbomole. *Wiley Interdiscip. Rev. Comput. Mol. Sci.* **2014**, *4*, 91–100. [CrossRef]
30. Weigend, F.; Häser, M. RI-MP2: First derivatives and global consistency. *Theor. Chem. Acc.* **1997**, *97*, 331–340. [CrossRef]
31. Haase, F.; Ahlrichs, R. Semidirect MP2 gradient evaluation on workstation computers: The MPGRAD program. *J. Comput. Chem.* **1993**, *14*, 907–912. [CrossRef]
32. Ghahremanpour, M.M.; Van Maaren, P.J.; Ditz, J.C.; Lindh, R.; Van Der Spoel, D. Large-scale calculations of gas phase thermochemistry: Enthalpy of formation, standard entropy, and heat capacity. *J. Chem. Phys.* **2016**, *145*, 114305. [CrossRef]
33. Grimme, S. Improved second-order Møller–Plesset perturbation theory by separate scaling of parallel- and antiparallel-spin pair correlation energies. *J. Chem. Phys.* **2003**, *118*, 9095–9102. [CrossRef]
34. Dunning, T.H. Gaussian basis sets for use in correlated molecular calculations. I. The atoms boron through neon and hydrogen. *J. Chem. Phys.* **1989**, *90*, 1007–1023. [CrossRef]
35. Weigend, F.; Häser, M.; Patzelt, H.; Ahlrichs, R. RI-MP2: Optimized auxiliary basis sets and demonstration of efficiency. *Chem. Phys. Lett.* **1998**, *294*, 143–152. [CrossRef]
36. Hättig, C.; Schmitz, G.; Kossmann, J. Auxiliary basis sets for density-fitted correlated wavefunction calculations: Weighted core-valence and ECP basis sets for post-d elements. *Phys. Chem. Chem. Phys.* **2012**, *14*, 6549–6555. [CrossRef] [PubMed]
37. Bushmarinov, I.; Lyssenko, K.A.; Antipin, M.Y. Atomic energy in the ‘Atoms in Molecules’ theory and its use for solving chemical problems. *Russ. Chem. Rev.* **2009**, *78*, 283–302. [CrossRef]
38. Johnson, E.R.; Keinan, S.; Mori-Sánchez, P.; Contreras-García, J.; Cohen, A.J.; Yang, W. Revealing Noncovalent Interactions. *J. Am. Chem. Soc.* **2010**, *132*, 6498–6506. [CrossRef] [PubMed]
39. Lu, T.; Chen, F. Multiwfn: A multifunctional wavefunction analyzer. *J. Comput. Chem.* **2012**, *33*, 580–592. [CrossRef]
40. Espinosa, E.; Molins, E.; Lecomte, C. Hydrogen bond strengths revealed by topological analyses of experimentally observed electron densities. *Chem. Phys. Lett.* **1998**, *285*, 170–173. [CrossRef]
41. Hanson, R.M. Jmol— a paradigm shift in crystallographic visualization. *J. Appl. Crystallogr.* **2010**, *43*, 1250–1260. [CrossRef]
42. Ramasubbu, N.; Parthasarathy, R.; Murray-Rust, P. Angular preferences of intermolecular forces around halogen centers: Preferred directions of approach of electrophiles and nucleophiles around carbon-halogen bond. *J. Am. Chem. Soc.* **1986**, *108*, 4308–4314. [CrossRef]
43. Lommerse, J.P.M.; Stone, A.J.; Taylor, R.; Allen, F.H. The Nature and Geometry of Intermolecular Interactions between Halogens and Oxygen or Nitrogen. *J. Am. Chem. Soc.* **1996**, *118*, 3108–3116. [CrossRef]
44. Wilcken, R.; Zimmermann, M.O.; Lange, A.; Joerger, A.C.; Boeckler, F.M. Principles and Applications of Halogen Bonding in Medicinal Chemistry and Chemical Biology. *J. Med. Chem.* **2013**, *56*, 1363–1388. [CrossRef]
45. Erdélyi, M. Halogen bonding in solution. *Chem. Soc. Rev.* **2012**, *41*, 3547–3557. [CrossRef] [PubMed]
46. Politzer, P.; Murray, J.S.; Clark, T. Halogen bonding and other σ -hole interactions: A perspective. *Phys. Chem. Chem. Phys.* **2013**, *15*, 11178–11189. [CrossRef]
47. Metrangolo, P.; Murray, J.S.; Pilati, T.; Politzer, P.; Resnati, G.; Terraneo, G. The fluorine atom as a halogen bond donor, viz. a positive site. *CrystEngComm* **2011**, *13*, 6593–6596. [CrossRef]
48. Bader, R.F.W. Bond Paths Are Not Chemical Bonds. *J. Phys. Chem. A* **2009**, *113*, 10391–10396. [CrossRef] [PubMed]
49. Shahbazian, S. Why Bond Critical Points Are Not “Bond” Critical Points. *Chem. A Eur. J.* **2018**, *24*, 5401–5405. [CrossRef] [PubMed]